RESEARCH ARTICLE
PLANETARY SCIENCES

Earth and Planetary Physics
4: 51–61, 2020
doi: 10.26464/epp2020002

Upstream proton cyclotron waves: occurrence and amplitude dependence on IMF cone angle at Mars — from MAVEN observations

Di Liu[1,2], ZhongHua Yao[1,2,3], Yong Wei[1,2*], ZhaoJin Rong[1,2], LiCan Shan[1], Stiepen Arnaud[3], Espley Jared[4], HanYing Wei[5], and WeiXing Wan[1,2]

[1]Key Laboratory of Earth and Planetary Physics, Institute of Geology and Geophysics, Chinese Academy of Sciences, Beijing 100029, China;

[2]College of Earth and Planetary Sciences, University of Chinese Academy of Sciences, Beijing 100049, China;

[3]Laboratoire de Physique Atmospherique et Planetaire, STAR institute, Universite de Liege, Liege, Belgium;

[4]NASA Goddard Space Flight Center, Greenbelt, Maryland, USA;

[5]Department of Earth, Planetary and Space Sciences, University of California, Los Angeles, California, USA

Key Points:

- The number of observed PCW events decreases exponentially with increasing event duration
- PCW amplitudes tend to decrease slightly with increasing IMF cone angle
- Upstream PCWs at Mars occur more frequently at intermediate IMF cone angles, a result that is not influenced by our temporal selection of MAVEN data for purposes of this study

Citation: Liu, D., Yao, Z. H., Wei, Y., Rong, Z. J., Shan, L. C., Arnaud, S., Jared, E., Wei, H. Y., and Wan, W. X. (2020). Upstream proton cyclotron waves: occurrence and amplitude dependence on IMF cone angle at Mars — from MAVEN observations. *Earth Planet. Phys.*, *4*(1), 51–61. http://doi.org/10.26464/epp2020002

Abstract: Proton cyclotron waves (PCWs) can be generated by ion pickup of Martian exospheric particles in the solar wind. The solar wind ion pickup process is highly dependent on the "IMF cone angle" — the angle between the solar wind velocity and the interplanetary magnetic field (IMF), which also plays an important role in the generation of PCWs. Using data from 2.15 Martian years of magnetic field measurements collected by the Mars Atmosphere and Volatile Evolution (MAVEN) mission, we have identified 3307 upstream PCW events. Their event number distribution decreases exponentially with their duration. A statistical investigation of the effects of IMF cone angle on the amplitudes and occurrence rates of PCWs reveals a slight tendency of PCWs' amplitudes to decrease with increasing IMF cone angle. The relationship between the amplitude and IMF cone angle is weak, with a correlation coefficient $r = -0.3$. We also investigated the influence of IMF cone angle on the occurrence rate of PCWs and found that their occurrence rate is particularly high for intermediate IMF cone angles (~18°–42°) even though highly oblique IMF orientation occurs most frequently in the upstream region of the Martian bow shock. We also conclude that these variabilities are not artefacts of temporal coverage biases in MAVEN sampling. Our results demonstrate that whereas IMF cone angle strongly influences the occurrence of PCWs, IMF cone angle may also weakly modulate their amplitudes in the upstream region of Mars.

Keywords: ion pickup; proton cyclotron waves; Martian exosphere

1. Introduction

For a planet such as Mars without a global intrinsic magnetic field, solar wind interacts directly with the planetary exosphere and subsequently causes exospheric neutrals to escape from the planet in a particular physical way, i.e., by ion pickup. In this process, neutral atoms can be ionized via photo-ionization, electron impact ionization, or charge exchange processes (Zhang et al., 1993). The newborn ions are further accelerated by solar wind convection electric field and will eventually be assimilated into the rapidly moving solar wind (Yoon and Wu CS, 1991). At Mars, due to the small size of the bow shock (subsolar shock distance at ~1.5R_M from the center of Mars), the hydrogen exosphere extends beyond the bow shock; neutral atoms from the exosphere can thus be picked up at distances of several planetary radii from the planet (Yamauchi et al., 2015).

It has been suggested that such newborn ions produced in the pickup process, especially protons, may constitute a significant non-thermal component of the total solar wind ion distribution function, which is unstable and can provide free energy to generate various plasma instabilities (Wu CS and Davidson, 1972; Wu CS and Hartle, 1974). The IMF cone angle $\alpha_{V,B}$, which is the angle

Correspondence to: Y. Wei, weiy@mail.iggcas.ac.cn
Received 15 OCT 2019; Accepted 11 NOV 2019.
Accepted article online 26 DEC 2019.

between the solar wind velocity and the IMF direction, is a key parameter in determining what type of instability may grow (Tsurutani and Smith, 1986; Tsurutani et al., 1987). When the IMF cone angle $\alpha_{V,B} = 0°$, newborn ions form a cold beam that interacts with the solar wind via the electromagnetic ion/ion right-hand (RH) resonant instability in the solar wind frame (Gary et al., 1984, and references therein). At the opposite extreme, $\alpha_{V,B} = 90°$, newborn ions form a ring in velocity space that can drive instability in the electromagnetic ion/ion left-hand (LH) mode. If $0° < \alpha_{V,B} < 90°$, newborn ions correspond to ring-beam distributions which can drive either or both RH and LH instabilities. At relatively small values of this angle, the RH mode is the dominant ion/ion mode with a maximum growth rate that increases with $\alpha_{V,B}$ (Gary and Madland, 1988). At sufficiently large values of $\alpha_{V,B}$, the LH mode appears, with growth rates that, similarly, increase as $\alpha_{V,B}$ increases (Gary and Madland, 1988). Based on computer simulations of wave growth generated by fresh pickup ions, the critical value of $\alpha_{V,B}$ at which the RH mode has the larger maximum growth rate, can be different. For instance, Brinca and Tsurutani (1989) have suggested this typical value to be around 75°, whereas Gary and Madland (1988) shows that RH mode can have larger maximum growth rate than LH mode up to $\alpha_{V,B} = 90°$. In the spacecraft frame, different wave modes are observed left-handed and at a frequency very close to the local proton gyrofrequency, due to the Doppler shift effect associated with the relative velocity between the spacecraft and the solar wind (Brinca, 1991). Therefore, the waves with frequencies close to the local proton gyrofrequency are called proton cyclotron waves (PCWs).

PCWs at Mars were first reported in Russell et al. (1990), based on observations from the Phobos mission. They proposed a hypothesis that the waves were related to the solar wind picking up newly-ionized hydrogen atoms from the Martian exosphere. Their hypothesis was later confirmed by Barabash et al. (1991). Subsequent studies on PCWs were made based on Mars Global Surveyor (MGS) observations (e.g., Brain et al., 2002; Mazelle et al., 2004; Wei HY and Russell, 2006; Romanelli et al., 2013; Bertucci et al., 2013; Wei HY et al., 2011, 2014) and the recent MAVEN mission (Connerney et al., 2015a; Romanelli et al., 2016), in which the recorded waves are at about the local proton gyrofrequency, left-hand polarized, and propagating quasi-parallel with respect to the IMF. Venus has a plasma environment similar to that of Mars; PCWs have been identified at the upstream of Venus (Delva et al., 2008, 2011). Moreover, PCWs have also been reported in the magnetospheres of Jupiter and Saturn (Blanco-Cano et al., 2001; Leisner et al., 2006; Russell et al., 2016; Meek et al., 2016; etc.), and at comets (Tsurutani, 1991; Mazelle and Neubauer, 1993).

It is generally believed that PCW amplitudes are determined primarily by the number and kinetic energy of newborn ions, and by the fraction of kinetic energy that is lost to the waves during the wave growth. As a result, wave activity could also be used to diagnose local exospheric neutral densities and ion production rates (Huddleston et al., 1998; Cowee et al., 2007). Numerical simulations of wave generation excited by newborn ions, for varying plasma conditions and IMF cone angles, have been widely explored (e.g., Gary et al., 1984; Winske and Gary, 1986; Gary et al., 1988; Gary et al., 1989; Cowee et al., 2012). Among these studies, Gary et al. (1988) simulated the case for $\alpha_{V,B} = 0°$ and showed that the energy density of magnetic field fluctuations is a function of local plasma parameters, particularly the ion injection rate. Gary et al. (1989) extended these results to nonzero $\alpha_{V,B}$ and showed that the peak amplitude of magnetic field fluctuation during wave growth is proportional to $\cos^8(\alpha_{V,B})$ when $0° < \alpha_{V,B} < 45°$. Cowee et al. (2012) suggested that the relation between local ion cyclotron wave amplitudes and local ion pickup rates can be influenced by multiple key factors, i.e., the growth time of the instability, non-uniform ion production rates, and the injection angles of newborn ions. In recent years, observations from the MAG instruments onboard MGS and MAVEN also invited studies of these waves. The wave amplitudes were found to decrease with radial distance from Mars, indicating that Mars is the source of these waves (Wei HY and Russell, 2006; Romanelli et al., 2013; Wei HY et al., 2014). Moreover, Romanelli et al. (2013) found a decreasing tendency of the wave amplitudes with increasing IMF cone angle, based on data from the MGS Science Phasing Orbits (SPO). However, Wei HY et al. (2014) did not observe such a decreasing tendency in data collected during the first aerobreaking phase (AB1) of MGS. Linear theory predicts that, in addition to affecting wave amplitudes, the IMF cone angle should also affect the linear growth rate of the waves (Gary, 1993). Analyzing MGS data, Wei HY et al. (2014) found that the waves occur more frequently for intermediate IMF cone angles, with the largest occurrence rate at around 45°. Romanelli et al. (2016) first confirmed the previously reported long-term temporal variability in the occurrence rate of PCWs (Romanelli et al., 2013; Bertucci et al., 2013) with MAG measurements from MAVEN; they related the temporal variabilities of PCW abundance to changes of hydrogen exospheric densities on the Martian dayside. Their study has comprehensively discussed the temporal changes in PCW abundance, but does not address sufficiently the influence of the IMF cone angle; although IMF cone angle plays a significant role in the generation of waves excited by newborn ions, there is no agreement as to the effect of IMF cone angle on wave characteristics, particularly on wave amplitudes that are essential to estimating local ion pickup rates.

In the present work, we use MAVEN's high-resolution magnetic field data to characterize upstream PCWs and study comprehensively the influence of IMF cone angle. The MAVEN mission was launched in November 2013 and arrived at Mars in September 2014. Its orbit has a nominal periapsis altitude of 150 km, an apoapsis altitude of 6220 km, and a period of about 4.5 hours (Jakosky et al., 2015). The orbit was designed in such a way that the apoapsis is located at times in the undisturbed solar wind upstream from the bow shock, and at other times inside the induced magnetosphere. When the spacecraft apoapsis is located upstream from the bow shock, upstream measurements can be obtained for typically 4 to 5 months. In between these 4- to 5-month time segments we lose the upstream coverage for typically 2 months because of the precession of the spacecraft apoapsis to the night side. Thus, MAVEN's orbit enables us to obtain a large number of measurements in the upstream region, which is ideal for studying upstream phenomena at Mars. We use MAVEN data spanning approximately 2.15 Martian years to investigate the two important characteristics of PCWs, i.e., their amplitudes and occurrence rates. We focus mainly on the impact of IMF cone angle on these two characteristics. The present work is structured as fol-

lows. In Section 2 we show a typical example of PCWs detected by MAG and the statistics of these PCWs. In Section 3 we present statistical analyses of the influence of IMF cone angle on the amplitude and occurrence rate of these waves. Finally, our findings and conclusions appear in Section 4.

2. Observations

2.1 Data Description

The MAG instrument onboard MAVEN is a fluxgate magnetometer that provides vector magnetic field measurements over a broad range (to 65536 nT per axis) at a sampling cadence of 32 Hz and accuracy of 0.25 nT (Connerney et al., 2015b). To investigate the relatively low frequency of PCWs (0.06 Hz for IMF values ~4 nT), we have resampled MAG data from 32 Hz to 1 Hz. We also used the MAVEN Solar Wind Ion Analyzer (SWIA) to extract upstream solar wind parameters. SWIA is a toroidal electrostatic analyzer that measures ion fluxes and ion moments over a broad energy range (from 10 eV to 25 keV) with a sampling cadence of 4 s (Halekas et al., 2015). We use here the onboard-calculated moments of the ion distribution functions to measure the solar wind velocity, at a time resolution of 4 seconds.

2.2 PCW Observations on 07 January 2017

Here we show an example of a PCW event in the upstream region

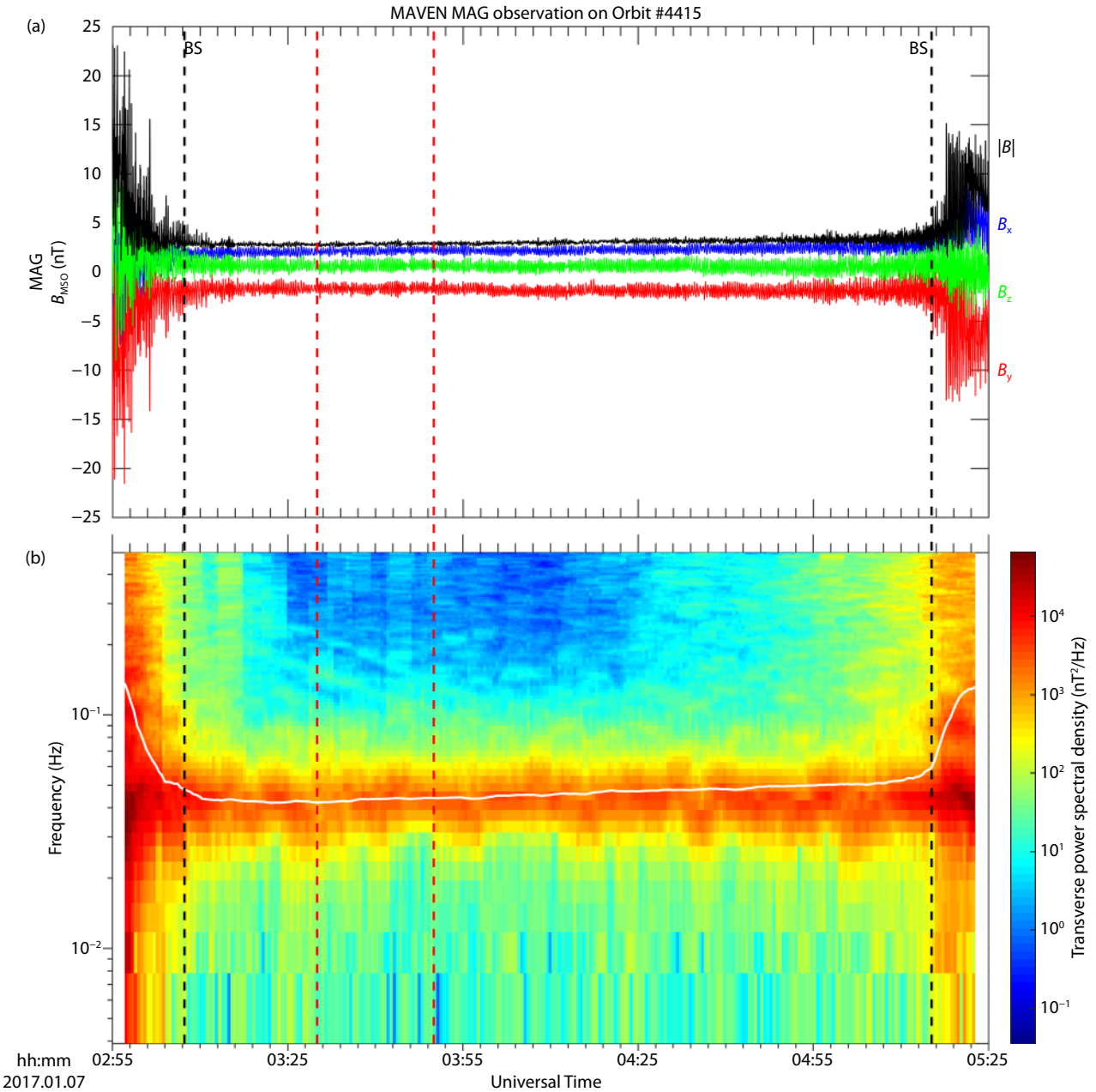

Figure 1. Proton cyclotron wave event observed by MAVEN on January 07, 2017. The location of the bow shock in this orbit is marked by black dashed lines; the subinterval marked by red dashed lines is analyzed in Figure 2. (a) The 1-Hz magnetic field in MSO coordinates observed by MAG; (b) Dynamic Fourier spectra of the transverse power derived from the MAG data, with the local proton gyrofrequency marked by white line.

of Mars. Figure 1a presents the 1-Hz magnetic field measurements in Mars-centered Solar Orbital (MSO) coordinates during MAVEN orbit 4415 on 07 January 2017. The MSO coordinate system is defined as follows: the *X* axis points toward the Sun, the *Z* axis is perpendicular to Mars's orbital plane and positive toward the ecliptic north, and the *Y* axis completes the right-handed system. In this time interval (02:55–05:25 UT), MAVEN was mainly in the upstream solar wind and crossed the bow shock (BS) at 03:07:20 UT and 05:15:15 UT, respectively, as indicated by the vertical black dashed lines. The mean IMF during the upstream period was [2.25, −2.22, 0.66] nT. Figure 1b shows the dynamic Fourier spectra of the transverse power, which is calculated by summing powers of magnetic field B_X component and B_Y component in the field-aligned (FA) coordinate system, which is defined as follows: the +*Z* axis is defined as the direction of the mean magnetic field during a period of time (in this study, typically ten local proton cyclotron periods); two vectors perpendicular to the mean-field direction complete the right-handed coordinate system. The compressional power given by the power from the B_Z component is not shown in Figure 1 since PCWs are predominantly transverse waves. As seen in Figure 1b, distinctive wave fluctuations in the vicinity of the local proton gyrofrequency (indicated by the white line in Figure 1b) were observed during the entire upstream solar wind period of the orbit.

To investigate the wave properties, we apply a wave analysis program to the magnetic field data collected during the subinterval 03:30–03:50 UT (indicated by the red dashed lines in Figure 1) based on the Means method (Means, 1972). Using the information contained in the imaginary part of the covariance matrix of the magnetic field, the Means method is able to analyze the polarization properties of plane waves, such as direction of propagation, ellipticity, and polarization. Notably, the Means method is superior to other methods in determining the sense of wave polarization. The calculations of the wave parameters are explicitly indicated in Means (1972) and Eqs. (20) and (23) in Rankin and Kurtz (1970), respectively. More details about the Means method can be found in these references.

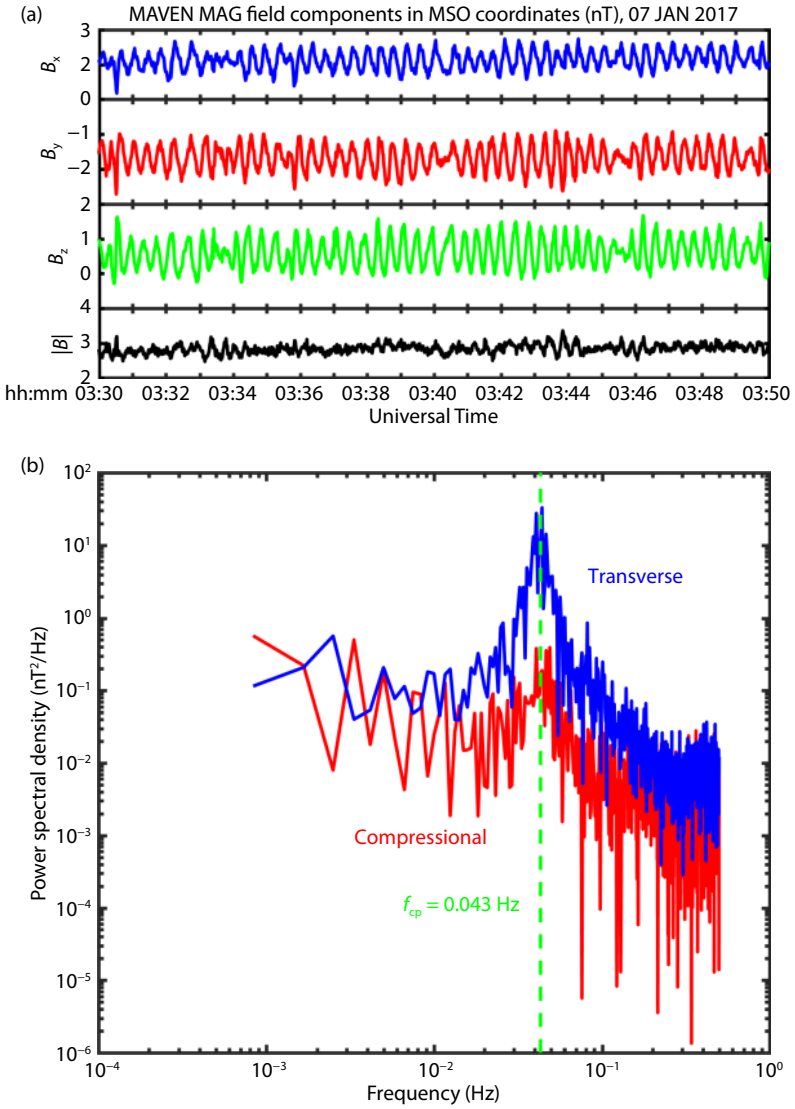

Figure 2. Proton cyclotron waves during the subinterval 03:30–03:50 UT, as indicated by the red dashed lines in Figure 1. (a) Magnetic field measured by MAVEN; (b) Power spectrum of time series shown in Figure 2a; the green line indicates the local proton gyrofrequency.

Figure 2a shows the 1-Hz magnetic field in MSO coordinates during the subinterval 03:30–03:50 UT, and Figure 2b displays the power spectral density for both the compressional and transverse components. As seen in Figure 2b, the wave was identified as mainly transverse (i.e., the transverse power was about two orders higher than the compressional power at the local proton gyrofrequency) with a narrow peak frequency at around the local proton gyrofrequency, f_{cp} (i.e., 0.043 Hz in this case; $f_{cp} = \frac{q|B|}{2\pi m}$, where $|B|$ is the averaged magnetic field magnitude). From the wave analysis based on the Means method, the wave is found to be left-handed with an ellipticity of –0.85, and to exhibit a polarization of 0.97 and a propagating direction of 15° with respect to the mean background magnetic field. The event has an amplitude of 0.36 nT and an averaged IMF cone angle $\alpha_{V,B}$ of ~41°. The wave amplitude is determined from the transverse power spectral density in a frequency interval $[0.8f_{cp}, 1.2f_{cp}]$. The IMF cone angle $\alpha_{V,B}$ was defined as $\alpha_{V,B} = \cos^{-1}(|\boldsymbol{x}\cdot\boldsymbol{b}|)$, where $\boldsymbol{x}$ denotes the unit vector of the solar wind velocity and $\boldsymbol{b}$ denotes the unit vector of the magnetic field. The solar wind velocity vectors were derived from the SWIA moments data. To survey the general properties of PCWs as a function of cone angle, a statistical study is performed based on MAG measurements in the following.

2.3 Statistics of PCWs

To identify all the PCW events during more than two Martian years, we first examined the MAG data taken in November 2014 and selected all the PCW events manually, according to the theoretical predications and the selection criteria in previous work (Wei HY et al., 2014). By analyzing the properties of these PCW events, we determined the following specific selection criteria: (1) the ratio of the transverse power to compressional power is greater than 1.5 and the transverse power derived within 20% of the local proton gyrofrequency is enhanced, i.e. the enhanced power peak is at least roughly 2 times larger than its neighbor power; (2) the wave is left-handed with ellipticity less than –0.7; (3) the percent polarization is greater than 70%; (4) the propagation angle with respect to the average magnetic field is smaller than 30 degrees. In this work, we first determine the Martian upstream region by analyzing manually the combined observations of magnetic field and plasma data. Then we apply these four criteria to the public MAG data collected only during the following eight time periods, during which MAVEN had upstream coverage: 30 October 2014 to 19 March 2015, 3 June 2015 to 5 November 2015, 2 December 2015 to 13 April 2016, 26 May 2016 to 10 October 2016, 29 November 2016 to 1 April 2017, 20 May 2017 to 30 September 2017, 23 November 2017 to 3 May 2018 and 13 June 2018 to 14 November 2018. Using the criteria described above, we identified automatically 3307 upstream PCW events for the statistical study. Figure 3 shows the histogram of the duration of these PCW observations in units of local proton cyclotron period. The durations of the observed waves range from 3 local proton gyroperiods up to about 500 local proton gyroperiods. The number of PCW events observed decreases exponentially with increasing duration, with a least square fitted function of $N = 2604e^{-0.0396x}$ where x is in units of local proton cyclotron period (red line in Figure 3). The goodness-of-fit is 0.99. A total of 3307 PCWs are represented in the distribution; the durations of 52.9% of the events were less than 20 local proton gyroperiods.

Figure 4 displays the spatial distribution of PCW amplitudes averaged in each $0.1R_M \times 0.1R_M$ bin in cylindrical MSO coordinates. The

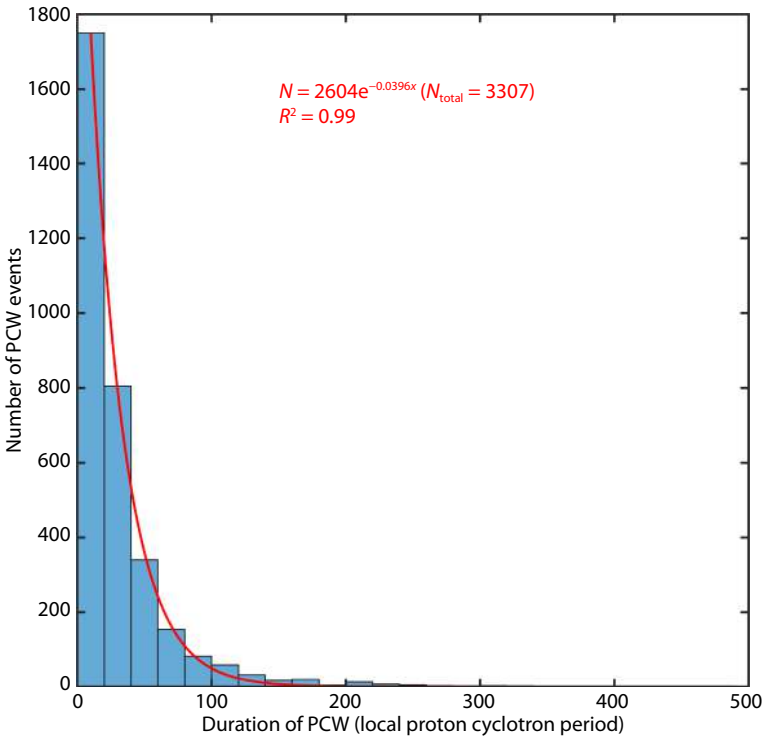

Figure 3. Histogram of the duration of PCWs in 20 local proton cyclotron period bins. The red line marks the least square fitted function $N = 2604e^{-0.0396x}$, where x is in units of local proton cyclotron period.

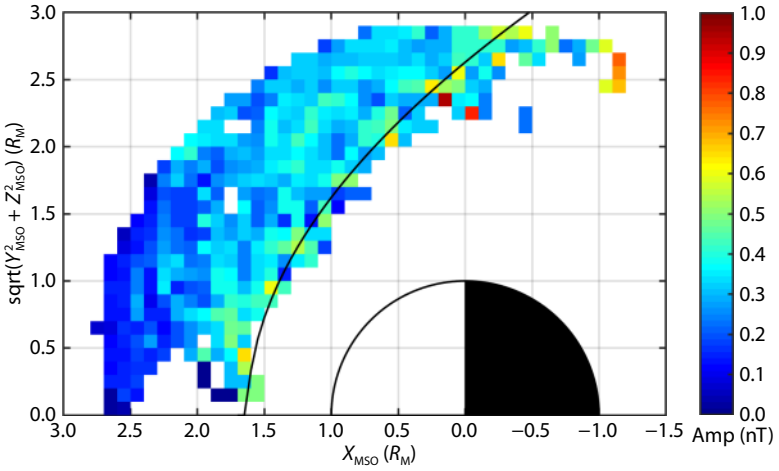

Figure 4. Spatial distribution of PCW amplitudes, averaged in each $0.1R_M \times 0.1R_M$ bin. The black solid line marks the bow shock location from the empirical model of Trotignon et al. (2006) and color coding is wave amplitude.

coordinate system is centered on Mars with the *X* axis pointing to the Sun and the rho axis pointing radially outward from the *X* axis. The color coding represents the amplitude of PCWs. $0.1R_M \times 0.1R_M$ bin resolution ensures us a good statistical study and allows us to obtain a reasonably good spatial variation, although other similar bin resolutions may also work well. The typical bow shock location from the empirical model of Trotignon et al. (2006) is marked by the black curve.

According to Figure 4, we find that the wave amplitudes are nearly constant in the region we observed. In order to study variations of amplitude with altitude, we also applied a linear regression (not shown here) involving the altitude. To eliminate the effect of the IMF cone angle, we divided all events into different groups according to IMF cone angles. Applying linear regression to each group of events within the same cone-angle range we find that the variations of amplitude with altitude are negligible. In particular, the amplitude remains nearly constant in the altitude range of 2–3R_M, which is the main region in which the PCWs studied here were observed to occur. Previous studies based on MGS data (Wei HY and Russell, 2006; Romanelli et al., 2013; Wei HY et al., 2014) have reported that the wave amplitudes decrease slowly with radial distance from the planet, however this tendency could not be confirmed in our results since the spatial coverage of MGS and MAVEN are different. MAVEN's altitude coverage is no more than 2R_M whereas MGS can detect up to 15R_M during its AB1 phase. This means that the key factor in controlling PCW amplitude — pickup ion density, may not change significantly within the region in which data analyzed in this study were collected. However, the rich data collected by MAVEN in such a narrow altitude range was ideal for our purpose, which was to study the effect of IMF cone angle on PCW amplitude without the complication of the influence on wave amplitudes of distance from Mars.

3. IMF Influence on PCWs

3.1 IMF Influence on PCWs' Amplitude

Figure 5 shows the amplitude of the waves as a function of IMF cone angle. The gray dots correspond to the amplitude of each PCW event. The red curve represents the median amplitudes with error bars of upper and lower quartiles calculated in ten cone angle bins, which have cone angle of 0°–26°, 26°–34°, 34°–40°, 40°–46°, 46°–51°, 51°–56°, 56°–61°, 61°–66°, 66°–73°, 73°–90° degree. The bin size was chosen to ensure approximately equal numbers of cases in each bin. From the median values displayed in the figure, we note that the amplitude of the PCWs has tendency to decrease as the IMF cone angle increases, from 0.34 nT at cone angle of ~20° to 0.16 nT at cone angle of ~80°. However, the data points are largely scattered, so we performed a statistical analysis to evaluate the reliability of the effect of IMF cone angle on wave amplitudes. The Spearman correlation coefficient $r = -0.3$ indicates that the correlation between IMF cone angle and wave amplitudes is very weak. Thus, based on the statistical results, we suggest that PCWs' amplitudes have at most a small and slightly decreasing dependence on IMF cone angle; moreover, the amplitudes vary very slowly with IMF cone angle, even though the median values display a descending trend. The significant scattering in Figure 5 indicate that the relationship between wave amplitudes and IMF cone angle is weak, or there exist other major factors contributing to wave amplitude growth, which will be addressed in the discussion section.

3.2 IMF Influence on PCWs' Occurrence

IMF cone angle, besides affecting PCW amplitudes, also determines the velocity distribution of pickup ions, which could control the type of instability, as we have previously mentioned. To investigate which cone angle conditions most favor PCW generation at Mars, we calculated the occurrence rate of PCWs as a function of IMF cone angle. In this work, we have folded the angle $\alpha_{V,B}$ between 90° and 180° into 0°–90° (i.e., $\alpha_{V,B}$=180°–$\alpha_{V,B}$ when $\alpha_{V,B}$ is greater than 90°), since linear theory indicates that it is the angle between the direction of both vectors but not the sense of them that affects wave growth (see, e.g., Gary, 1993). Figure 6a shows a histogram for all 60-s-averaged IMF cone angle data in upstream solar wind, regardless of wave activity; Figure 6b shows the same histogram as Figure 6a but only for times when PCWs were observed. The dashed lines in Figure 6a and Figure 6b represent the median values in the two groups. The occurrence rate for each cone angle bin shown in Figure 6c is derived by dividing Figure 6b

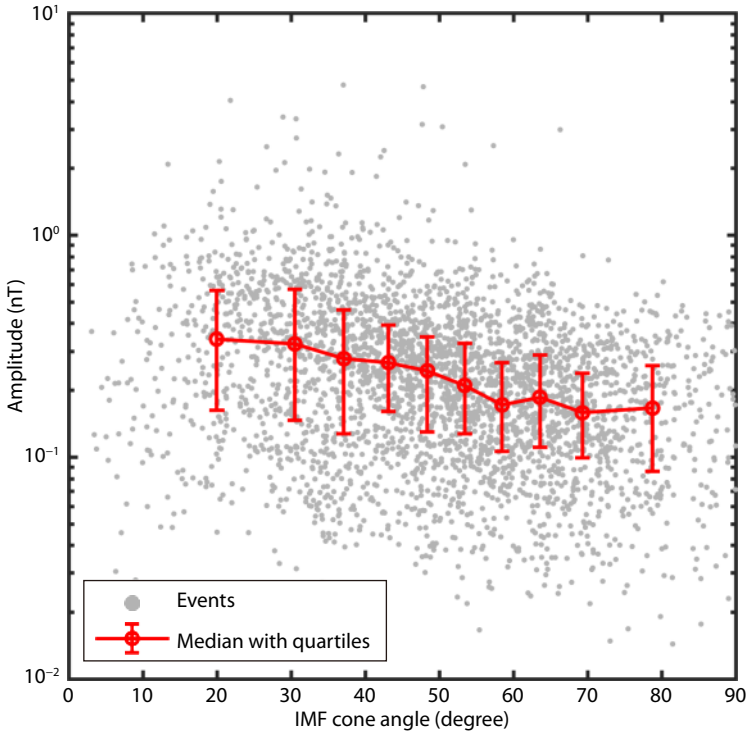

Figure 5. PCW amplitudes as a function of IMF cone angle, for all upstream wave events. The red circles mark the medians with error bars of upper and lower quartiles in each cone angle bin.

by Figure 6a. Although the IMF is more oblique from the solar wind velocity at Mars, PCWs tend to occur more often at medium IMF cone angles and less frequently at large IMF cone angles. The PCW occurrence rate reaches its highest value at the cone angle range of ~18°–42°, and then decreases slowly as the cone angle increases from ~42° to ~72°.

Previous studies have reported a temporal variability of the occurrence of PCWs observed upstream of Mars, indicating that PCWs occur more frequently around the time of perihelion/southern summer solstice than at the times of spring and autumn equinoxes, a trend similar to those of Martian dayside hydrogen exospheric density and the solar extreme ultraviolet (EUV) flux at the Martian environment (Bertucci et al., 2013; Romanelli et al., 2016). Thus, seasonal changes in solar EUV heating and ultimately hydrogen exospheric density also have an impact on wave occurrence. To investigate whether the changes of PCW occurrence for various IMF cone angles are relevant to seasonal changes, we examine whether there are significant differences in MAVEN's temporal sampling at different IMF cone angles. We first sort all the eight time periods into two groups, according to the solar longitude (Ls): time periods close to the Martian perihelion (PH, Ls = 251°) with high PCWs occurrence rate (containing 30 October 2014 to 19 March 2015, 26 May 2016 to 10 October 2016, 29 November 2016 to 1 April 2017 and 13 June 2018 to 14 November 2018) and time periods close to the Martian aphelion (APH, Ls = 71°) with low PCWs occurrence rate (containing 3 June 2015 to 5 November 2015, 2 December 2015 to 13 April 2016, 20 May 2017 to 30 September 2017 and 23 November 2017 to 3 May 2018). Then in Figure 7 we plot the distributions of these two groups as a function of IMF cone angle; the red bar represents the percentage of time periods close to the Martian PH and the blue bar represents the same detail for the Martian APH. As can be seen in the histogram, the distribution for different IMF cone angles are similar to each other, showing approximately no asymmetry for any IMF cone angle range. For various IMF cone angles, the percentage of PH time periods remains nearly constant at around 0.55, slightly higher than the percentage of APH time periods, 0.45. This comparison therefore also suggests that temporal variabilities in the occurrences of PCWs cannot be the reason for the observed relationship between IMF cone angle and PCW occurrence rate.

4. Discussion and Conclusions

In this paper, we have first determined how IMF cone angle influences upstream PCW amplitudes, based on MAG data from 2.15 Martian years of the MAVEN mission (10 October 2014 to 14 November 2018). After excluding variations of PCW amplitude caused by radial distance from Mars, we found a slight tendency of PCW amplitude to decrease as IMF cone angle increases. This result is consistent with the observations of Romanelli et al. (2013). Using MAG data collected during the MGS SPO phase, they reported a slight shift toward smaller amplitudes as the IMF cone angle increased. Interestingly, Wei HY et al. (2014) found no clear variation in wave amplitude with IMF cone angle during the first aerobreaking phase (AB1) of MGS. Indeed, upstream PCWs observed in Wei HY et al. (2014) could extend as far as $15R_M$ beyond the bow shock, which may lead to a rapidly changing pickup ion density and ultimately to the absence of wave amplitude dependence on IMF cone angle. Therefore, the difference between the results in Wei HY et al. (2014) and Romanelli et al. (2013) could be due to the different spatial coverages sampled by MGS during

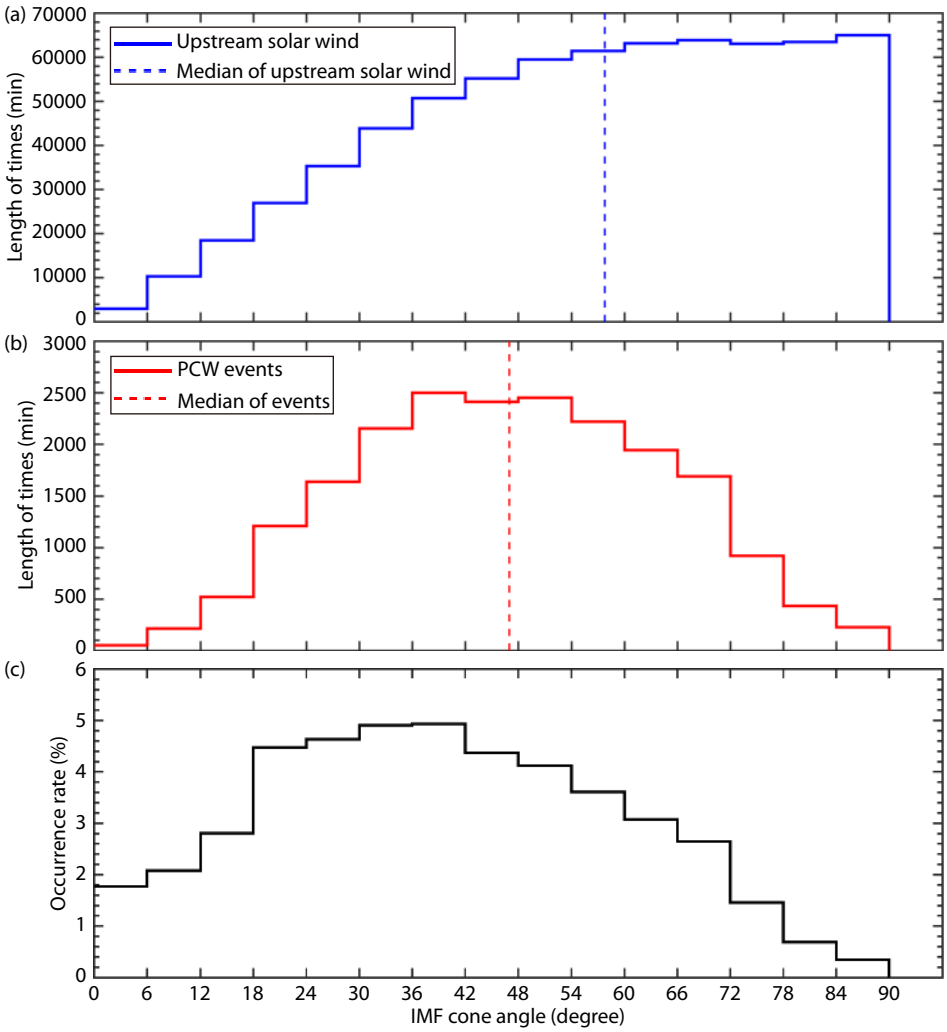

Figure 6. (a) Histogram of IMF cone angles for upstream solar wind (blue solid line); the vertical blue dashed line denotes the median value; (b) Histogram of IMF cone angles for wave events (red solid line); the vertical red dashed line denotes the median value; (c) Occurrence rate of PCWs.

AB1 vs. SPO. In this study, the data we used were collected in the altitude range of 1.5R_M–3R_M; our result is thus comparable with that of Romanelli et al. (2013). This result could be explained by theoretical predictions and numerical simulations of the generation of the waves excited by newborn ions. Nonlinear theories predict that the pickup ions will lose more energy to the waves in the instance of pure "beam"-driven instability (RH mode) than in the case of pure "ring"-driven instability (LH mode) (Winske and Gary, 1986), leading to a lower saturation energy for smaller drift velocity ($V_{SW}\cos\alpha_{V,B}$) of newborn ions (Gary et al., 1988). Gary et al. (1989) simulated the magnetic fluctuation level for varying IMF cone angles and showed that, if other plasma parameters such as pickup ion production rate are fixed, the peak amplitude of magnetic field fluctuation during wave growth is proportional to $\cos^8(\alpha_{V,B})$ at $0° < \alpha_{V,B} < 45°$. Moreover, Cowee et al. (2012) carried out an analysis of the evolution of wave energy, assuming varying pickup ion production rates and IMF cone angles, using the 1D hybrid simulation of the Martian plasma environment. Their simulation results indicated that for relatively high ion production rates (higher than 10^{-4}cm^{-3}s^{-1} with a radial distance smaller than 5R_M from Mars), the saturation wave energy is highest for $\alpha_{V,B} = 0°$, and then decreases as $\alpha_{V,B}$ increases. In our work, the spatial distribution of PCWs events is limited in the region within the radial distance range of 1.5–3.0R_M, which means that for such relatively high ion production rates, the saturation wave energies in the region should decrease with increasing $\alpha_{V,B}$. The amplitudes of the waves at other planets were also discussed. Inside Jupiter and Saturn's magnetospheres, pickup ions generally form a "ring" distribution in velocity space (pickup angle is 90°) since the corotating plasmas in Jupiter and Saturn's magnetospheres are moving nearly perpendicularly to the ambient magnetic field. Cowee et al. (2007) carried out 1D hybrid simulations of SO_2^+ ring instability in the Io plasma torus and predicted that, for conditions at Io, at most ~25% of the energy of the newborn ion population is lost to wave growth. In contrast to newborn ion driven instability in the magnetospheres of Jupiter or Saturn, newborn ions in cometary environments, where larger amplitude waves are often observed, are picked up into the solar wind and may form parallel drifting beams. Cowee et al. (2007) thus simulated the beam driven instability in a cometary environment and found that such instability releases ~30% of the initial newborn ion beam energy to wave growth, demonstrating that "beam"-driven instability can lose

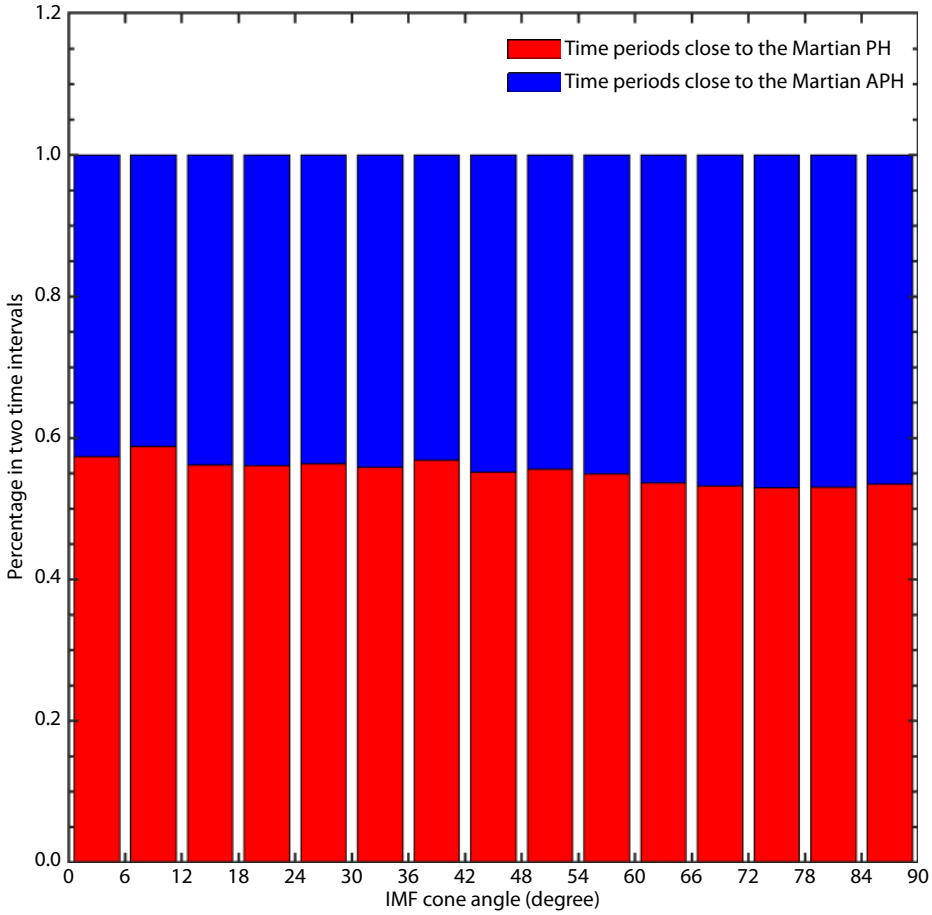

Figure 7. The percentage of MAVEN sampling in two groups as a function of IMF cone angle. The two groups contain time periods close to the Martian PH (red bar) and time periods close to the Martian APH (blue bar), respectively.

more energy to wave growth than "ring"-driven instability. At comet Giacobini-Zinner, Tsurutani et al. (1989) reported the absence of large amplitude magnetic fluctuation near the water-group gyrofrequency for conditions when $\alpha_{V,B}$ is near 90°.

However, due to the large scattering of data points in Figure 5, the correlation between PCWs' amplitudes and IMF cone angle is not strong enough to be statistically significant. We suggest that the unsaturated state of PCWs at Mars could account for this result. Despite the fact that the saturation wave energy will reach a higher level for smaller IMF cone angle, as theoretical considerations and simulations have suggested, PCWs are not always observed at a saturated state, but more often in a state of wave growth (Cowee et al., 2012). Once the exospheric hydrogen atoms are ionized, the newborn ions are strongly influenced by IMF and solar wind convection electric field, forming a non-Maxwellian velocity distribution, which provides the free energy to generate instabilities. After initial ionization, a significant time may be required before observable wave fluctuations develop. For example, the simulation results in Cowee et al. (2012) suggest that, assuming a nominal ion production rate (3.4×10^{-4} cm^{-3}s^{-1}), about 10 cyclotron periods (equivalent to 230 s for the case in Figure 1) are required before saturation occurs for $\alpha_{V,B}$ = 0°. If we further assume that the waves are being transported past Mars with the solar wind velocity at ~ 400 km/s, they would travel a distance of $27R_M$ in 10 ion cyclotron periods, which is much farther than the length of the mass-loading region. Within such a large region, the non-uniform pickup ion production rates are insufficient to feed the waves, and the particles can also be scattered by the bow shock or assimilated into the solar wind and swept away into the interplanetary space. Therefore, the detectable waves in the upstream region are mostly in a state of growth, which explains the wide range of scattering in the amplitudes of PCWs seen in Figure 5.

We would also like to point out that signals from the spacecraft reaction wheels can be detected by the magnetometer as low amplitude signals (~0.1 nT) (Connerney et al., 2015a) at variable but narrow frequencies of ~0.5 and ~1.5 Hz. However, since these reaction wheel signals only rarely match our PCW selection criteria (e.g. registering within 20% of the local gyrofrequency), these non-environmental signals should have an insignificant impact on our statistical results.

Furthermore, we have determined the occurrence rate of PCWs as a function of IMF cone angle based on the MAVEN data. We find that PCWs tend to occur more often at medium IMF cone angles (~18°–42°) and less frequently at large IMF cone angles, even though the IMF is more oblique from the solar wind velocity in the upstream region of the Martian bow shock. We also conclude that these variabilities are not associated with biases of temporal coverage of MAVEN sampling. The preference of occurrence at intermediate IMF cone angles is also found in Wei HY et al., (2014). We

infer that the preference for intermediate IMF cone angles is a consequence of wave growth rate under different IMF cone angles and pickup ion densities. For small IMF cone angles, although the waves can reach a relatively high magnetic fluctuation level as explained above, more time is needed to reach a detectable level since the growth rate of the instability increases as $\alpha_{V,B}$ increases (Gary and Madland, 1988), which lowers the detectability of PCWs. For large IMF cone angles, although wave growth rates are larger and times required to reach saturation are shorter than for small angles, the saturation wave energy is lower than that for small angles. This means that the waves for large IMF cone angles can be detected by the spacecraft only when the pickup ion density is high enough to generate sufficiently high magnetic fluctuation levels. As a result, stricter conditions need to be satisfied for wave generation when the cone angle is highly oblique, which naturally reduces the observed occurrence rate. Therefore, only for intermediate IMF cone angles does wave growth require relatively short times and modest pickup ion densities, so that a high probability of detection is expected.

Acknowledgments

The MAVEN data used in this paper are publicly available in NASA's Planetary Data System (http://ppi.pds.nasa.gov/mission/). The authors would like to thank J. E. P. Connerney for helpful suggestions. This work was supported by the Strategic Priority Research Program of Chinese Academy of Sciences (Grant No. XDA17010201). This work was supported by Thousand Young Talents Program of China and Chinese NSFC grant (41525016, 41474155, 41661164034, 41621004, 41374180, 41774188). Z. H. Y is a Marie-Curie COFUND research fellow, cofunded by EU. A. Stiepen is supported by the Fund for Scientific Research (F.R.S.-FNRS).

References

Barabash, S., Dubinin, E., Pissarenko, N., Lundin, R., and Russell, C. T. (1991). Picked-up protons near Mars: PHOBOS observations. *Geophys. Res. Lett.*, *18*(10), 1805–1808. https://doi.org/10.1029/91GL02082

Bertucci, C., Romanelli, N., Chaufray, J. Y., Gomez, D., Mazelle, C., Delva, M., Modolo, R., González-Galindo, F., and Brain, D. A. (2013). Temporal variability of waves at the proton cyclotron frequency upstream from Mars: implications for Mars distant hydrogen exosphere. *Geophys. Res. Lett.*, *40*(15), 3809–3813. https://doi.org/10.1002/grl.50709

Blanco-Cano, X., Russell, C. T., Huddleston, D. E., and Strangeway, R. J. (2001). Ion cyclotron waves near Io. *Planet. Space Sci.*, *49*(10-11), 1125–1136. https://doi.org/10.1016/S0032-0633(01)00020-4

Brain, D. A., Bagenal, F., Acuña, M. H., Connerney, J. E. P., Crider, D. H., Mazelle, C., Mitchell, D. L., and Ness, N. F. (2002). Observations of low-frequency electromagnetic plasma waves upstream from the Martian shock. *J. Geophys. Res.*, *107*(A6), 1076. https://doi.org/10.1029/2000JA000416

Brinca, A. L., and Tsurutani, B. T. (1989). Influence of multiple ion species on low-frequency electromagnetic wave instabilities. *J. Geophys. Res.*, *94*(A10), 13565–13569. https://doi.org/10.1029/JA094iA10p13565

Brinca, A. L. (1991). Cometary linear instabilities: from profusion to perspective. In A. Johnstone (Ed.), *Cometary Plasma Processes* (pp. 211-221). Washington, DC: American Geophysical Union. https://doi.org/10.1029/GM061p0211

Connerney, J. E. P., Espley, J. R., DiBraccio, G. A., Gruesbeck, J. R., Oliversen, R. J., Mitchell, D. L., Halekas, J., Mazelle, C., Brain, D., and Jakosky, B. M. (2015a). First results of the MAVEN magnetic field investigation. *Geophys. Res. Lett.*, *42*(21), 8819–8827. https://doi.org/10.1002/2015GL065366

Connerney, J. E. P., Espley, J., Lawton, P., Murphy, S., Odom, J., Oliversen, R., and Sheppard, D. (2015b). The MAVEN magnetic field investigation. *Space Sci. Rev.*, *195*(1-4), 257–291. https://doi.org/10.1007/s11214-015-0169-4

Cowee, M. M., Winske, D., Russell, C. T., and Strangeway, R. J. (2007). 1D hybrid simulations of planetary ion-pickup: energy partition. *Geophys. Res. Lett.*, *34*(2), L02113. https://doi.org/10.1029/2006GL028285

Cowee, M. M., Gary, S. P., and Wei, H. Y. (2012). Pickup ions and ion cyclotron wave amplitudes upstream of Mars: first results from the 1D hybrid simulation. *Geophys. Res. Lett.*, *39*(8), L08104. https://doi.org/10.1029/2012GL051313

Delva, M., Zhang, T. L., Volwerk, M., Magnes, W., Russell, C. T., and Wei, H. Y. (2008). First upstream proton cyclotron wave observations at Venus. *Geophys. Res. Lett.*, *35*(3), L03105. https://doi.org/10.1029/2007GL032594

Delva, M., Mazelle, C., Bertucci, C., Volwerk, M., Vörös, Z., and Zhang, T. L. (2011). Proton cyclotron wave generation mechanisms upstream of Venus. *J. Geophys. Res.*, *116*(A2), A02318. https://doi.org/10.1029/2010JA015826

Gary, S. P., Smith, C. W., Lee, M. A., Goldstein, M. L., and Forslund, D. W. (1984). Electromagnetic ion beam instabilities. *Phys. Fluids*, *27*(7), 1852–1862. https://doi.org/10.1063/1.864797

Gary, S. P., and Madland, C. D. (1988). Electromagnetic ion instabilities in a cometary environment. *J. Geophys. Res.*, *93*(A1), 235–241. https://doi.org/10.1029/JA093iA01p00235

Gary, S. P., Madland, C. D., Omidi, N., and Winske, D. (1988). Computer simulations of two-pickup-ion instabilities in a cometary environment. *J. Geophys. Res.*, *93*(A9), 9584–9596. https://doi.org/10.1029/JA093iA09p09584

Gary, S. P., Akimoto, K., and Winske, D. (1989). Computer simulations of cometary-ion/ion instabilities and wave growth. *J. Geophys. Res.*, *94*(A4), 3513–3525. https://doi.org/10.1029/JA094iA04p03513

Gary, S. P. (1993). *Theory of Space Plasma Microinstabilities*. Cambridge, UK: Cambridge University Press.

Halekas, J. S., Taylor, E. R., Dalton, G., Johnson, G., Curtis, D. W., McFadden, J. P., Mitchell, D. L., Lin, R. P., and Jakosky, B. M. (2015). The solar wind ion analyzer for MAVEN. *Space Sci. Rev.*, *195*(1-4), 125–151. https://doi.org/10.1007/s11214-013-0029-z

Huddleston, D. E., Strangeway, R. J., Warnecke, J., Russell, C. T., and Kivelson, M. G. (1998). Ion cyclotron waves in the Io torus: wave dispersion, free energy analysis, and SO_2^+ source rate estimates. *J. Geophys. Res.*, *103*(E9), 19887–19899. https://doi.org/10.1029/97JE03557

Jakosky, B. M., Lin, R. P., Grebowsky, J. M., Luhmann, J. G., Mitchell, D. F., Beutelschies, G., Priser, T., Acuna, M., Andersson, L., … Brain, D. (2015). The Mars Atmosphere and Volatile Evolution (MAVEN) mission. *Space Sci. Rev.*, *195*(1-4), 3–48. https://doi.org/10.1007/s11214-015-0139-x

Leisner, J. S., Russell, C. T., Dougherty, M. K., Blanco-Cano, X., Strangeway, R. J., and Bertucci, C. (2006). Ion cyclotron waves in Saturn's E ring: initial Cassini observations. *Geophys. Res. Lett.*, *33*(11), L11101. https://doi.org/10.1029/2005GL024875

Mazelle, C., and Neubauer, F. M. (1993). Discrete wave packets at the proton cyclotron frequency at Comet P/Halley. *Geophys. Res. Lett.*, *20*(2), 153–156. https://doi.org/10.1029/92GL02613

Mazelle, C., Winterhalter, D., Sauer, K., Trotignon, J. G., Acuña, M. H., Baumgärtel, K., Bertucci, C., Brain, D. A., Brecht, S. H., … Slavin, J. (2004). Bow shock and upstream phenomena at Mars. *Space Sci. Rev.*, *111*(1-2), 115–181. https://doi.org/10.1023/B:SPAC.0000032717.98679.d0

Means, J. D. (1972). Use of the three-dimensional covariance matrix in analyzing the polarization properties of plane waves. *J. Geophys. Res.*, *77*(28), 5551–5559. https://doi.org/10.1029/JA077i028p05551

Meeks, Z., Simon, S. and Kabanovic, S. (2016). A comprehensive analysis of ion cyclotron waves in the equatorial magnetosphere of Saturn. *Planet. Space Sci.*, *129*, 47–60. https://doi.org/10.1016/j.pss.2016.06.003

Rankin, D., and Kurtz, R. (1970). Statistical study of micropulsation polarizations. *J. Geophys. Res.*, *75*(28), 5444–5458. https://doi.org/10.1029/JA075i028p05444

Romanelli, N., Bertucci, C., Gómez, D., Mazelle, C., and Delva, M. (2013). Proton cyclotron waves upstream from Mars: observations from Mars global surveyor. *Planet. Space Sci.*, *76*, 1–9. https://doi.org/10.1016/j.pss.2012.10.011

Romanelli, N., Mazelle, C., Chaufray, J. Y., Meziane, K., Shan, L., Ruhunusiri, S., Connerney, J. E. P., Espley, J. R., Eparvier, F., … Jakosky, B. M. (2016). Proton cyclotron waves occurrence rate upstream from Mars observed by MAVEN: associated variability of the Martian upper atmosphere. *J. Geophys. Res.*, *121*(11), 11113–11128. https://doi.org/10.1002/2016JA023270

Russell, C. T., Luhmann, J. G., Schwingenschuh, K., Riedler, W., and Yeroshenko, Y. (1990). Upstream waves at Mars: Phobos observations. *Geophys. Res. Lett.*, *17*(6), 897–900. https://doi.org/10.1029/GL017i006p00897

Russell, C. T., Wei, H. Y., Cowee, M. M., Neubauer, F. M., and Dougherty, M. K. (2016). Ion cyclotron waves at Titan. *J. Geophys. Res.*, *121*(3), 2095–2103. https://doi.org/10.1002/2015JA022293

Trotignon, J. G., Mazelle, C., Bertucci, C., and Acuña, M. H. (2006). Martian shock and magnetic pile-up boundary positions and shapes determined from the Phobos 2 and Mars Global Surveyor data sets. *Planet. Space Sci.*, *54*(4), 357–369. https://doi.org/10.1016/j.pss.2006.01.003

Tsurutani, B. T., and Smith, E. J. (1986). Strong hydromagnetic turbulence associated with comet Giacobini-Zinner. *Geophys. Res. Lett.*, *13*(3), 259–262. https://doi.org/10.1029/GL013i003p00259

Tsurutani, B. T., Thorne, R. M., Smith, E. J., Gosling, J. T., and Matsumoto, H. (1987). Steepened magnetosonic waves at comet Giacobini-Zinner. *J. Geophys. Res.*, *92*(A10), 11074–11082. https://doi.org/10.1029/JA092iA10p11074

Tsurutani, B. T., Page, D. E., Smith, E. J., Goldstein, B. E., Brinca, A. L., Thorne, R. M., Matsumoto, H., Richardson, I. G., and Sanderson, T. R. (1989). Low-frequency plasma waves and ion pitch angle scattering at large distances (3.5×10^5 km) from Giacobini-Zinner: interplanetary magnetic field α dependences. *J. Geophys. Res.*, *94*(A1), 18–28. https://doi.org/10.1029/JA094iA01p00018

Tsurutani, B. T. (1991). Comets: a laboratory for plasma waves and instabilities. In A. Johnstone (Ed.), *Cometary Plasma Processes* (pp. 189-209). Washington, DC: American Geophysical Union. https://doi.org/10.1029/GM061p0189

Wei, H. Y., and Russell, C. T. (2006). Proton cyclotron waves at Mars: exosphere structure and evidence for a fast neutral disk. *Geophys. Res. Lett.*, *33*(23), L23103. https://doi.org/10.1029/2006GL026244

Wei, H. Y., Russell, C. T., Zhang, T. L., and Blanco-Cano, X. (2011). Comparative study of ion cyclotron waves at Mars, Venus and Earth. *Planet. Space Sci.*, *59*(10), 1039–1047. https://doi.org/10.1016/j.pss.2010.01.004

Wei, H. Y., Cowee, M. M., Russell, C. T., and Leinweber, H. K. (2014). Ion cyclotron waves at Mars: occurrence and wave properties. *J. Geophys. Res.*, *119*(7), 5244–5258. https://doi.org/10.1002/2014JA020067

Winske, D., and Gary, S. P. (1986). Electromagnetic instabilities driven by cool heavy ion beams. *J. Geophys. Res.*, *91*(A6), 6825–6832. https://doi.org/10.1029/JA091iA06p06825

Wu, C. S., and Davidson, R. C. (1972). Electromagnetic instabilities produced by neutral–particle ionization in interplanetary space. *J. Geophys. Res.*, *77*(28), 5399–5406. https://doi.org/10.1029/JA077i028p05399

Wu, C. S., and Hartle, R. E. (1974). Further remarks on plasma instabilities produced by ions born in the solar wind. *J. Geophys. Res.*, *79*(1), 283–285. https://doi.org/10.1029/JA079i001p00283

Yamauchi, M., Hara, T., Lundin, R., Dubinin, E., Fedorov, A., Sauvaud, J. A., Frahm, R. A., Ramstad, R., Futaana, Y., …Barabash, S. (2015). Seasonal variation of Martian pick-up ions: Evidence of breathing exosphere. *Planet. Space Sci.*, *119*, 54–61. https://doi.org/10.1016/j.pss.2015.09.013

Yoon, P. H., and Wu, C. S. (1991). Ion pickup by the solar wind via wave-particle interactions. In A. Johnstone (Ed.), *Cometary Plasma Processes* (pp. 241-258). Washington, DC: American Geophysical Union. https://doi.org/10.1029/GM061p0241

Zhang M. H. G., Luhmann, J. G., Nagy, A. F., Spreiter, J. R., and Stahara, S. S. (1993). Oxygen ionization rates at Mars and Venus: relative contributions of impact ionization and charge exchange. *J. Geophys. Res.*, *98*(E2), 3311–3318. https://doi.org/10.1029/92JE02229